A combination mode of the annual cycle and the El Nino/ Southern Oscillation

Author:
Stuecker, Malte F.; Timmermann, Axel; Jin, Fei-Fei; McGregor, Shayne; Ren, Hong-Li

Publication details:
Nature Geoscience
v. 6
Chapter No. 7
pp. 540-544
1752-0894 (ISSN)

Publication Date:
2013

Publisher DOI:
http://dx.doi.org/10.1038/NGEO1826

A Combination Mode of Annual Cycle and the El Niño-Southern Oscillation

Malte F. Stuecker[1], Axel Timmermann[2], Fei-Fei Jin[1], Shayne McGregor[3,4] & Hong-Li Ren[1]

[1]*Department of Meteorology, SOEST, University of Hawai'i at Manoa, Honolulu, HI, USA.*

[2]*IPRC, SOEST, University of Hawai'i at Manoa, Honolulu, HI, USA.*

[3]*CCRC, University of New South Wales, Sydney, NSW, Australia.*

[4]*ARC Centre of Excellence for Climate System Science, University of New South Wales, Sydney, Australia.*

Atmospheric circulation anomalies associated with the interannual El Niño-Southern Oscillation (ENSO) phenomenon [1] exert global impacts on the climate system [2]. El Niño events are characterised by positive sea surface temperature anomalies in the eastern equatorial Pacific, whereas La Niña events exhibit an anomalously cold sea surface.

ENSO is considered an oscillatory instability of the tropical Pacific coupled ocean-atmosphere system [1,3–6]. The boreal winter peak of El Niño events and the seasonal variance modulation of associated eastern equatorial sea surface temperature anomalies [2], often referred to as phase-locking [7], document ENSO's tight interaction with the seasonal cycle.

To date there exists no established theory for ENSO's synchronisation with the annual cycle. In the present study, we show that seasonal changes in the western tropical Pacific warm pool region interact with El Niño, giving rise to a near-annual combination climate mode with periods of 10 and 15 months. Associated wind changes trigger the termination of large El

Niño events [8], thereby controlling ENSO's seasonal synchronisation and predictability. This combination mode is shown to cause massive shifts of Earth's largest rainbands, impacting human livelihoods across the Asia-Pacific region and beyond.

Current ENSO theories, such as the *Recharge Oscillator Paradigm* [9], while very successful in explaining some observational features of ENSO, do not account for the interaction between interannual and seasonal timescales. In particular, they do not provide any insight into why El Niño events peak toward the end of the calendar year (in December-January-February: DJF) and terminate in the subsequent months. Previous extensions to these theories that rely on nonlinear concepts [10–13], such as subharmonic frequency locking and frequency entrainment, nonlinear resonance, the quasi-periodic transition to chaos or parametric excitation [7,14,15], capture some aspects of ENSO / annual cycle interactions.

None of these extended dynamical systems' concepts, however, describe the observational finding [16] that a weakening and southward shift of westerly wind anomalies on the equator accompanies the termination of strong El Niño events. Numerous modelling studies [8,17–20] have confirmed this observational evidence, thus supporting the notion of strong annual cycle / ENSO interactions originating in the tropical western Pacific. Here, we set out to provide a simple unifying dynamical framework to understand various aspects of ENSO, such as the physics of seasonally-paced El Niño transitions, spectral characteristics and ENSO's hydroclimatic impacts.

The seasonal weakening and southward shift of westerly wind anomalies that contributes to the transition between El Niño and La Niña can be readily described in terms of an Empirical

Orthogonal Function (EOF) decomposition of the tropical wind anomaly field [8,21] for the observational period 1958-2001. The first EOF (EOF1) is the equatorially quasi-symmetric 10 m wind pattern associated with ENSO (Fig. 1a), featuring the anomalous Walker circulation, as characterised by equatorial westerly wind anomalies in the western Pacific (positive phase of the first Principal Component PC1, Fig. 1e) during El Niño. PC1 is well correlated (r=0.86) with the commonly used Niño 3.4 index (sea surface temperature (SST) anomalies averaged over 120°W-170°W and 5°S-5°N).

The second EOF (Fig. 1b), in combination with the positive phase of PC2 (termination phase of strong El Niño events, Fig. 1f) captures the development of the anomalous Philippine anticyclone [22], along with a strong meridional shear of anomalous zonal wind across the equator and a southward shifted westerly wind anomaly [8]. It plays an important role in terminating El Niño events [8] by re-establishing the upwelling regime in the equatorial eastern Pacific (the abrupt weakening of equatorial westerly wind anomalies triggers an upwelling Kelvin wave) and by discharging heat away from the equator into the Northern Hemisphere due to the off-equatorial wind stress curl pattern [8,23]. This is highlighted by the tight connection between PC1 and PC2 during the peak phase of strong El Niño events (Fig. 1e-f, Supplementary Fig. 3).

To further elucidate this connection between PC1 and PC2, the power spectra of the observed PCs are calculated (Fig. 2a, Supplementary Figs. 1a,2). The PC1 spectrum shows pronounced levels of variability mostly in the interannual period band of 2 - 8 years, in contrast to PC2 which exhibits a significant spectral peak at a period of $\sim$15 months and a weaker one at $\sim$10 months.

Transforming the frequency axis of the PC1 spectrum (hereafter represented by f) to $1 - f$ and $1 + f$, where 1 represents the annual frequency, we find that the peak of PC2 aligns well with the shifted $1 - f_{\mathrm{E}}$ peak of PC1, where f_{E} denotes the frequency band of ENSO (f_{E} = $\frac{1}{2}$ years^{-1} to $\frac{1}{8}$ years^{-1}). A multi-century long simulation with an ENSO-resolving coupled climate model captures the EOF2 pattern, PC2 time evolution, its phase relationship with PC1 and key spectral characteristics (Supplementary Figs. 6-10).

Spectral peaks at frequencies $1 - f_{\mathrm{E}}$ and/or $1 + f_{\mathrm{E}}$ on either side of the annual frequency are characteristics of near-annual *combination tones* (the difference and sum tone, respectively) that originate from an amplitude modulation of the annual cycle due to ENSO; or in mathematical terms from the product between ENSO and the annual cycle, or more complicated variants thereof. Combination tones were first described in acoustic theory during the 18^{th} and 19^{th} century [24,25]. Later, they were invoked to understand aspects of glacial cycles [26] and ENSO [13]. Near-annual spectral power has been identified in oceanic and atmospheric observations [22,27]. However, the exact physical origin and climatic relevance of these near-annual spectral peaks and the corresponding physical mode have so far gone unnoticed in studies of tropical climate.

Based on these spectral characteristics of wind PC2 we hypothesise that the mechanism responsible for seasonally-paced El Niño terminations is provided by a new *combination mode* (C-mode) of tropical Pacific climate. It emerges from the nonlinear interaction between seasonal cycle and interannual ENSO variability, primarily through an atmospheric nonlinearity, such as the nonlinear dissipation of momentum in the planetary boundary layer associated with the sea-

sonal development of the South Pacific Convergence Zone (SPCZ) [8] or the advection of low-level moisture.

To test this hypothesis we conduct a 10 member ensemble of sensitivity experiments with an Atmospheric General Circulation Model (AGCM), forced with only an SST seasonal cycle and time-evolving ENSO-related SST anomalies (EXP_A), associated with wind PC1. In addition, we conduct a single member experiment with the same ENSO SST forcing but without a seasonal cycle in SST (perpetual autumn equinox experiment PERP).

The AGCM-simulated ensemble mean wind EOF1 (Fig. 1c) reveals a very close similarity to the observed EOF1 (Fig. 1a) and high correlation between the corresponding PCs (r=0.95). The pronounced correspondence between simulated and observed EOF2 wind pattern (Fig. 1b,d) and the corresponding principal components during major El Niño events (Fig. 1f) confirms EOF2 as a C-mode resulting from the nonlinear interaction (product) between ENSO and the annual cycle. Moreover, the fact that the spatial structure of EOF2 is largely reproduced by this experiment further documents that the initiation of the Philippine anticyclone and the southward shift of the anomalous equatorial westerlies in DJF and their evolution in subsequent months are both manifestations of the nonlinear combination mode. The evolution of the simulated PC2 (Fig. 1f, Supplementary Fig. 3) documents a rapid transition at the end of the calendar year from negative to positive values during strong El Niño events, very similar to the observed PC2. The perpetual equinox experiment does not exhibit the characteristic atmospheric circulation response related to the combination mode (Supplementary Figs. 3,4), thus demonstrating that the annual cycle of SST

is a key element of the atmospheric combination mode response. Our results confirm and extend earlier modelling studies [17,18] that found that a fixed ENSO SST anomaly pattern together with an SST seasonal cycle were sufficient to simulate a southward shift of the ENSO-related wind anomalies in boreal winter and spring.

The power spectrum of the simulated ensemble PC2 average from $\mathrm{EXP_A}$ (Fig. 2b, Supplementary Fig. 1b), reveals combination tone frequency peaks at $1 - f_{\mathrm{E}}$ ($\sim$15 months) and $1 + f_{\mathrm{E}}$ ($\sim$10 months). As expected for a combination mode between ENSO and the annual cycle, we find a spectral gap for annual frequencies. In addition, we integrated the AGCM for 150 years with the annual cycle and ENSO-related SST anomalies ($\mathrm{EXP_B}$) obtained from EOF1 of a 500 year-long coupled pre-industrial control simulation (PICTRL). The results (Supplementary Figs. 6-10) show two very well pronounced spectral peaks for PC2 of the winds at combination tone frequencies. The two peaks match those from the fully coupled simulation (PC2 from PICTRL) and those from the shifted PC1 spectra of $\mathrm{EXP_B}$. The AGCM experiments ($\mathrm{EXP_A}$ and $\mathrm{EXP_B}$), the fully coupled model run PICTRL, and the observations, all exhibit very similar EOF2 wind structures (Fig. 1 b,d, Supplementary Fig. 6 b,d); however, there are slight differences in the prominence of spectral power in the $1 - f_{\mathrm{E}}$ and $1 + f_{\mathrm{E}}$ bands. These differences may be related to different representations of atmospheric nonlinearities and the reddening effect of air-sea coupling, which may act to favour a stronger $1 - f_{\mathrm{E}}$ peak over $1 + f_{\mathrm{E}}$. The power spectrum of the perpetual autumn equinox AGCM experiment neither exhibits the characteristic $1 - f_{\mathrm{E}}$ nor the $1 + f_{\mathrm{E}}$ combination tone frequency peaks in the PC2 spectra (Supplementary Fig. 5), thus supporting the evidence that the annual cycle in SST is a key component for the second EOF mode.

To further verify our combination mode hypothesis, we consider a theoretical approximation to the C-mode in the form of $\mathrm{PC1_{OBS}\,(t)} \times \cos\left(\omega_{\mathrm{a}}\mathrm{t} - \varphi\right)$, which comes from the lowest order term of the atmospheric nonlinearity. Here ω_a denotes the angular frequency of the annual cycle and φ represents a one month phase shift. This time series, labelled as $\mathrm{PC2_{SIMPLE}}$, by its mathematical nature, exhibits pronounced $1 - f_{\mathrm{E}}$ and $1 + f_{\mathrm{E}}$ spectral peaks (Fig. 2c, Supplementary Fig. 1c). Furthermore, it shows remarkable agreement with the observed PC2, especially during El Niño events (Fig. 1g, Supplementary Fig. 3). The correlation coefficient between $\mathrm{PC2_{SIMPLE}}$ and the observed PC2 is 0.51 and between $\mathrm{PC2_{SIMPLE}}$ and the averaged PC2 from experiment $\mathrm{EXP_A}$, is 0.67. The observed PC2 can thus be viewed as $\mathrm{PC2_{SIMPLE}}$ (Fig. 2c) superimposed on atmospheric white noise (Fig. 2b, Supplementary Fig. 11) and further reddened by air-sea coupling (Fig. 2a).

The seasonal development of the SPCZ in DJF has been previously shown to be a key element in generating the observed southward wind anomaly shift [8] during strong nonlinear El Niño events. During the 1982/83, 1991/92 and 1997/98 El Niño events the SPCZ collapsed into a zonal equatorial rainband with strongly increased precipitation on the equator and anomalous drying in the tropical north-west Pacific (Fig. 3a). These *zonal SPCZ events* [28,29] cause severe precipitation impacts in South Pacific Island Nations and influence Asian monsoon systems by changing the spatial distribution of diabatic heating. We find that C-mode dynamics are responsible for the spatial precipitation pattern during these events (Fig. 3c,d).

Summarising, in the present study we demonstrate that a series of climatic features occurring during the peak and termination phase of large El Niño events can be explained by a previously

overlooked near-annual combination mode resulting from the nonlinear interaction between seasonal and interannual SST forcing. These features include the Philippine anticyclone [22] (Fig. 1), zonal SPCZ events [28] (Fig. 3) and the southward shift of the westerly wind anomalies at the end of calendar year [16], which strongly contributes to the termination of large El Niño events [8].

Notably, the combination mode dynamics, as represented by PC2 of wind anomalies (Fig. 1e), occurs prominently for strong El Niño events and is less pronounced for weak El Niño events and La Niña events [21] . This amplitude asymmetry may explain why La Niña conditions are not characterised by a strong phase synchronisation with the seasonal cycle and why they can last for much longer than strong El Niño events discussed above (Fig. 1e). Once an El Niño event reaches a certain amplitude, its demise after DJF becomes highly predictable (Fig. 1g) and largely controlled by the C-mode. This contrasts the predictability of El Niño's onset phase, which is characterised by the stochastic occurrence of westerly wind bursts and other short-term phenomena [30]. Thus, studying this mode may help improve the ENSO performance in climate models and increase the skill of seasonal climate predictions.

Methods

Precipitation Analysis Using the Global Precipitation Climatology Project (GPCP V2.2) precipitation product for the period 1979-2000[S1], we reconstruct the anomalous austral summer precipitation fields for the three strongest wind PC2 anomaly events (1982/83, 1991/92, 1997/98) by multiplying the respective rainfall regression pattern with the DJF-mean values of the corresponding PCs (Fig. 3). Adding the anomalous rainfall associated just with PC1 during these events to the DJF-mean climatological rainfall results in an intensification of precipitation in some regions (Fig. 3b), but not the strong equatorial enhancement seen during zonal SPCZ events (Fig. 3a). Adding both the rainfall anomalies associated with the wind PC1 and PC2 (Fig. 3c) to the DJF-mean climatology results in the characteristic zonal orientation and eastward extension of zonal SPCZ events, very similar to the composite (Fig. 3a), as well as the north-western Pacific drying. This illustrates that the wind PC2 is an excellent indicator of zonal SPCZ events.

Combination Tones The two main nonlinear atmospheric processes in the tropical region are the dissipation of momentum in the planetary boundary layer and low-level moisture advection. These processes serve as exemplary sources of the atmospheric nonlinearity that can produce the combination tones. The anomalies in these two nonlinear processes give rise to anomalous momentum and moisture source terms containing $\vec{v}_A \cdot \vec{v}_E$ and $\vec{v}_A \cdot \nabla q_E + \vec{v}_E \cdot \nabla q_A$, respectively. Here $\vec{v}$ denotes horizontal velocity and ∇q the moisture gradient field. The subscripts A and E denote the fields associated with the annual cycle and ENSO respectively. If one considers simple sinusoid time evo-

lutions for these two source terms, these will be proportional to $A_A \cos(\omega_A t)\, A_E \cos(\omega_E t)$, where A_E and ω_E denote ENSO amplitude and angular frequency respectively and A_A and ω_A amplitude and angular frequency of the annual cycle. Thus, these kind of quadratic nonlinear processes allow ENSO to interact with the annual cycle to produce the sum and difference (combination) tones:

$$A_A \cos(\omega_A t)\, A_E \cos(\omega_E t) = \frac{1}{2} A_A A_E \left\{ \cos\left([\omega_A - \omega_E]\, t \right) + \cos\left([\omega_A + \omega_E]\, t \right) \right\}.$$

This mechanism operates in a similar way if we consider a frequency range for ENSO instead of a simple sinusoid.

$\mathrm{PC2}_{\mathrm{SIMPLE}}$ is the mathematical representation of the quadratic combination mode between ENSO (PC1) and the annual cycle. As such it serves as our base hypothesis. We show that PC2 $\mathrm{EXP_A}$ (Fig. 2b) is essentially $\mathrm{PC2}_{\mathrm{SIMPLE}}$ plus atmospheric white noise with a small red component (Supplementary Fig. 11). For consistency, we test both the observed and experiment PC2s against a red noise null hypothesis (Fig. 2a-b, Supplementary Fig. 1a-b). An additional test of PC2 $\mathrm{EXP_A}$ against white noise can be found in the supplementary material (Supplementary Fig. 11).

Full Methods (detailing the model experiments and spectral analysis) are available in the online supplementary material. Furthermore, it includes 11 additional figures and references S1-S26.

References

1. Philander, S. G. El Niño Southern Oscillation phenomena. *Nature* **302** (1983). Doi:10.1038/302295a0.

2. Rasmusson, E. M. & Carpenter, T. H. Variations in Tropical Sea Surface Temperature and Surface Wind Fields Associated with the Southern Oscillation/El Niño. *Mon. Wea. Rev.* **110**, 354–384 (1982). Doi:http://dx.doi.org/10.1175/1520-0493(1982)110¡0354:VITSST¿2.0.CO;2.

3. Cane, M. A. & Zebiak, S. E. A Theory for El Niño and the Southern Oscillation. *Science* **228**, 1085–1087 (1985). Doi:10.1126/science.228.4703.1085.

4. Jin, F.-F. Tropical Ocean-Atmosphere Interaction, the Pacific Cold Tongue, and the El Niño Southern Oscillation. *Science* **274**, 76–78 (1996). Doi:10.1126/science.274.5284.76.

5. Neelin, J. D. *et al.* ENSO theory. *J. Geophys. Res.* **103**, 14261–14290 (1998).

6. McPhaden, M. J., Zebiak, S. E. & Glantz, M. H. ENSO as an Integrating Concept in Earth Science. *Science* **314** (2006). Doi:10.1126/science.1132588.

7. Stein, K., Timmermann, A. & Schneider, N. Phase Synchronization of the El Niño-Southern Oscillation with the Annual Cycle. *Phys. Rev. Lett.* (2011). Doi:10.1103/PhysRevLett.107.128501.

8. McGregor, S., Timmermann, A., Schneider, N., Stuecker, M. F. & England, M. H. The effect of the South Pacific Convergence Zone on the termination of El Niño events and the meridional

asymmetry of ENSO. *J. Climate* **25**, 5566–5586 (2012). Doi: http://dx.doi.org/10.1175/JCLI-D-11-00332.1.

9. Jin, F.-F. An equatorial ocean recharge paradigm for ENSO. Part I: Conceptual model. *J. Atmos. Sci.* **54**, 811–829 (1997).

10. Jin, F.-F., Neelin, J. D. & Ghil, M. El Niño on the Devil's Staircase: Annual Subharmonic Steps to Chaos. *Science* **264**, 70–72 (1994). Doi:10.1126/science.264.5155.70.

11. Tziperman, E., Stone, L., Cane, M. & Jarosh, H. El Niño chaos: Overlapping of resonance between the seasonal cycle and the Pacific ocean-atmosphere oscillator. *Science* **264**, 72–74 (1994).

12. Chang, P., Wang, B., Li, T. & Ji, L. Interactions between the seasonal cycle and the Southern Oscillation - frequency entrainment and chaos in an intermediate coupled ocean-atmoshpere model. *Geophys. Res. Lett.* **21**, 2817–2820 (1994).

13. Jin, F.-F., Neelin, J. D. & Ghil, M. El Niño/Southern Oscillation and the annual cycle: subharmonic frequency-locking and aperiodicity. *Physica D* **98**, 442–465 (1996).

14. Thompson, C. J. & Battisti, D. S. A Linear Stochastic Dynamical Model of ENSO. Part I: Model Development. *J. Climate* **13**, 2818–2832 (2000).

15. An, S.-I. & Jin, F.-F. Linear solutions for the frequency and amplitude modulation of ENSO by the annual cycle. *Tellus A* **63** (2011).

16. Harrison, D. E. & Vecchi, G. A. On the termination of El Niño. *Geophys. Res. Lett.* **26**, 1593–1596 (1999).

17. Spencer, H. Role of the atmosphere in seasonal phase locking of El Niño. *Geophys. Res. Lett.* **31**, (2004). L24104, doi:10.1029/2004GL021619.

18. Vecchi, G. A. The Termination of the 1997-98 El Niño. Part II: Mechanism of Atmospheric Change. *J. Climate* **19**, 2647–2663 (2006).

19. Lengaigne, M., Boulanger, J.-P., Menkes, C. & Spencer, H. Influence of the Seasonal Cycle on the Termination of El Niño Events in a Coupled General Circulation Model. *J. Climate* **19**, 1850–1868 (2006).

20. Ohba, M. & Ueda, H. Role of Nonlinear Atmospheric Response to SST on the Asymmetric Transition Process of ENSO. *J. Climate* **22**, 177–192 (2009). Doi:10.1175/2008JCLI2334.1.

21. McGregor, S. *et al.* Meridional movement of wind anomalies during ENSO events and their role in event termination. *Geophys. Res. Lett.* (2013). Doi:10.1002/grl.50136.

22. Wang, B., Wu, R. & Lukas, R. Role of the Western North Pacific Wind Variation in Thermocline Adjustment and ENSO Phase Transition. *J. Meteor. Soc. Japan* **77**, 1–16 (1999).

23. Kug, J.-S., Kang, I.-S. & An, S.-I. Symmetric and antisymmetric mass exchanges between the equatorial and off-equatorial Pacific associated with ENSO. *J. Geophys. Res.-Oceans* **108** (2003). Doi:10.1029/2002JC001671.

24. Tartini, G. *Trattato di Musica secondo la vera scienza dell'armonia* (Padua, Italy: Univ. of Padua, 1754).

25. Helmholtz, H. L. F. *Die Lehre von den Tonempfindungen als physiologische Grundlage für die Theorie der Musik* (Friedrich Vieweg und Sohn, 1863).

26. Le Treut, H. & Ghil, M. Orbital Forcing, Climatic Interactions, and Glaciation Cycles. *J. Geophys. Res.* **88(C9)**, 5167–5190 (1983).

27. Ghil, M. & Robertson, A. W. Solving Problems with GCMs: General Circulation Models and Their Role in the Climate Modeling Hierarchy. In *General Circulation Model Development: Past, Present and Future*, 285–325 (Academic Press, 2000).

28. Cai, W. *et al.* More extreme swings of the South Pacific Convergence Zone due to greenhouse warming. *Nature* **488**, 365–369 (2012). Doi:10.1038/nature11358.

29. Vincent, E. M. *et al.* Interannual variability of the South Pacific Convergence Zone and implications for tropical cyclone genesis. *Clim. Dyn.* **36**, 1881–1896 (2011). Doi:10.1007/s00382-009-0716-3.

30. McPhaden, M. J. Genesis and Evolution of the 1997-98 El Niño. *Science* **283**, 950–954 (1999). Doi:10.1126/science.283.5404.950.

Supplementary Information is linked to the online version of the paper at www.nature.com/nature

Acknowledgements This study was supported by U.S. NSF grant ATM1034798, U.S. Department of Energy grant DESC005110, U.S. NOAA grant NA10OAR4310200, the 973 Program of China (2010CB950404) and the China Meteorological Special Project (GYHY201206033). A. T. additionally was supported by U.S. NSF grant 1049219 and through the Japan Agency for Marine-Earth Science and Technology (JAMSTEC) through its sponsorship of the International Pacific Research Center (IPRC). This is IPRC publication number 956 and SOEST contribution number 8889. We thank M. Ghil and two anonymous reviewers for their helpful comments.

Competing Interests The authors declare that they have no competing financial interests.

Author Contributions M. F. S., F.-F. J. and A. T. designed the study. M. F. S. conducted the experiments, performed the analysis and wrote the initial draft of the manuscript. All authors discussed the results and helped improving the manuscript.

Correspondence Correspondence and requests for materials should be addressed to F.-F. Jin (jff@hawaii.edu) or M. F. Stuecker (stuecker@soest.hawaii.edu).

Figure Captions

Figure 1 (a)-(d) Dominant pattern of wind variability (zonal wind as shading) in the tropical Pacific obtained by an EOF decomposition of 10 m wind anomalies. **(e)-(f)** Normalised PCs for observations (OBS) and experiment ($\mathrm{EXP_A}$). Blue boxes indicate duration (0.5σ threshold of PC1 OBS) of the four strongest El Niño events (determined by maximum PC1 OBS amplitude). Blue vertical lines highlight the event peak times. Grey boxes indicate duration (-0.5σ threshold of PC1 OBS) of the four strongest La Niña events (determined by minimum PC1 OBS amplitude). **(g)** The same as above but for PC2 OBS (solid black) and $\mathrm{PC2_{SIMPLE}}$ (solid orange).

Figure 2 Power spectra for PC1 and PC2 using the Blackman-Tukey (BT) method. Frequency is abbreviated by f. To illustrate the PC2 combination tone frequencies, PC1 was shifted to $1 - f$ (dashed blue) and $1 + f$ (dashed green) and scaled by a factor 1/3. Grey boxes indicate the near-annual combination tone frequency bands $1 - f_{\mathrm{E}}$ and $1 + f_{\mathrm{E}}$. The AR(1) null hypothesis for the PC2s in (a) and (b) is displayed by a thick grey line and the 95% confidence interval (CI) indicated by a thin grey line. **(a)** Observed PC1 and PC2. **(b)** Averaged experiment $\mathrm{EXP_A}$ PC1 and PC2. **(c)** Observed PC1 and $\mathrm{PC2_{SIMPLE}}$.

Figure 3 DJF-mean precipitation. The climatological DJF-mean 6 mm day^{-1} precipitation contour for the period 1979-2000 indicates the SPCZ extend during DJF (a-c). **(a)** Precipitation composite average for the three strongest PC2 anomaly events: 1982/83, 1991/92 and 1997/98. **(b)** Climatological precipitation plus the precipitation composite associated with the observed PC1 for these

events. **(c)** Climatological precipitation plus the precipitation composite associated with both observed PC1 and PC2 for these events. **(d)** Precipitation across 160°W (solid) and 120°W (dashed) for the panels (a)-(c): DJF composite (black), DJF climatology plus PC1 precipitation (blue) and DJF climatology plus PC1 and PC2 precipitation (red).

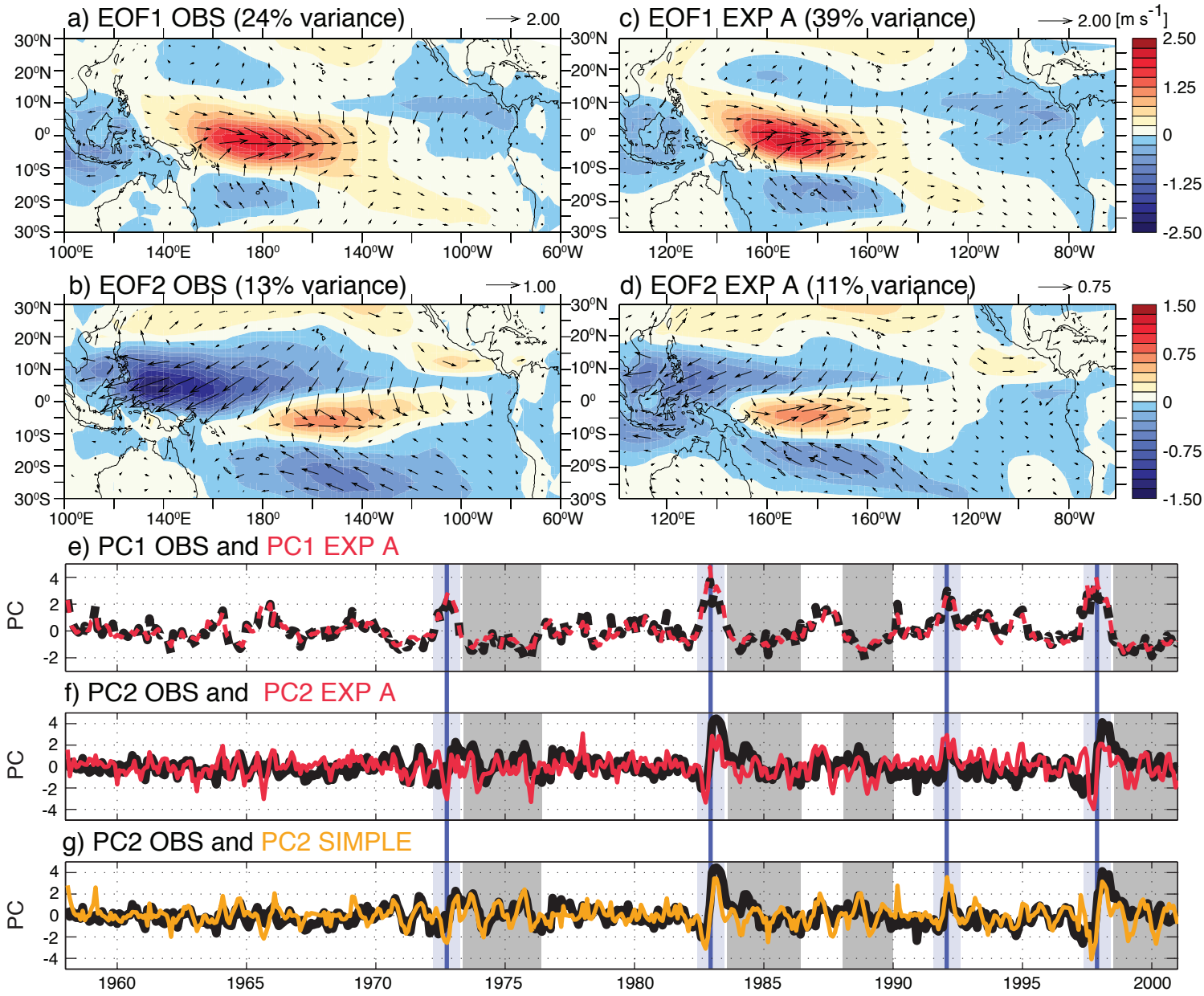
a) EOF1 OBS (24% variance)
2.00
c) EOF1 EXP A (39% variance)
2.00 [m s-1]
2.50
1.25
0
-1.25
-2.50
b) EOF2 OBS (13% variance)
1.00
d) EOF2 EXP A (11% variance)
0.75
1.50
0.75
0
-0.75
-1.50
30ºN
20ºN
10ºN
0º
10ºS
20ºS
30ºS
100ºE
140ºE
180º
140ºW
100ºW
60ºW
120ºE
160ºE
160ºW
120ºW
80ºW
e) PC1 OBS and PC1 EXP A
f) PC2 OBS and PC2 EXP A
g) PC2 OBS and PC2 SIMPLE
PC
4
2
0
-2
-4
1960
1965
1970
1975
1980
1985
1990
1995
2000

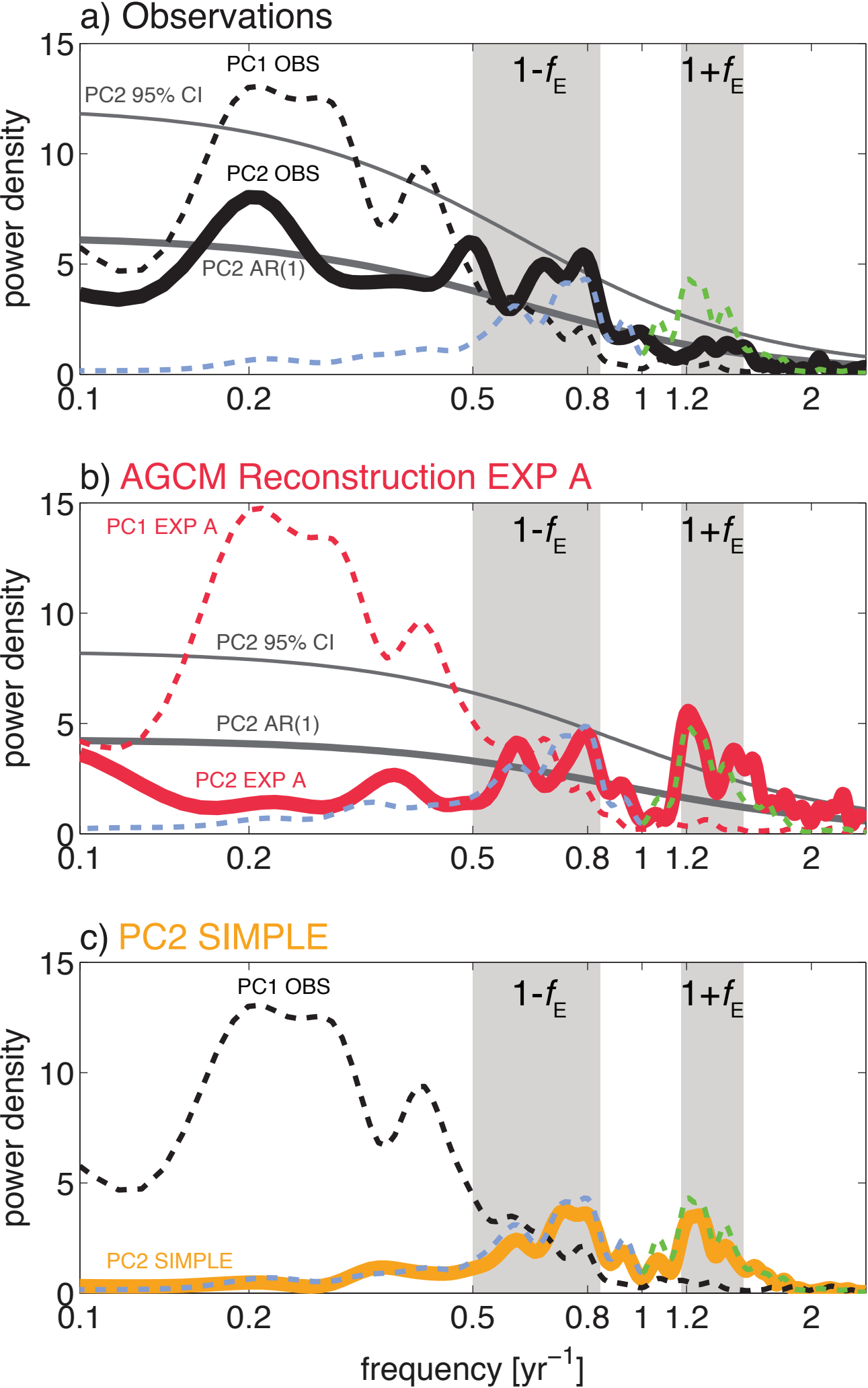
a) Observations
PC1 OBS
PC2 95% CI
PC2 OBS
PC2 AR(1)
1-f_E
1+f_E
power density
15
10
5
0
0.1
0.2
0.5
0.8
1
1.2
2
b) AGCM Reconstruction EXP A
PC1 EXP A
PC2 95% CI
PC2 AR(1)
PC2 EXP A
c) PC2 SIMPLE
PC1 OBS
PC2 SIMPLE
frequency [yr^{-1}]

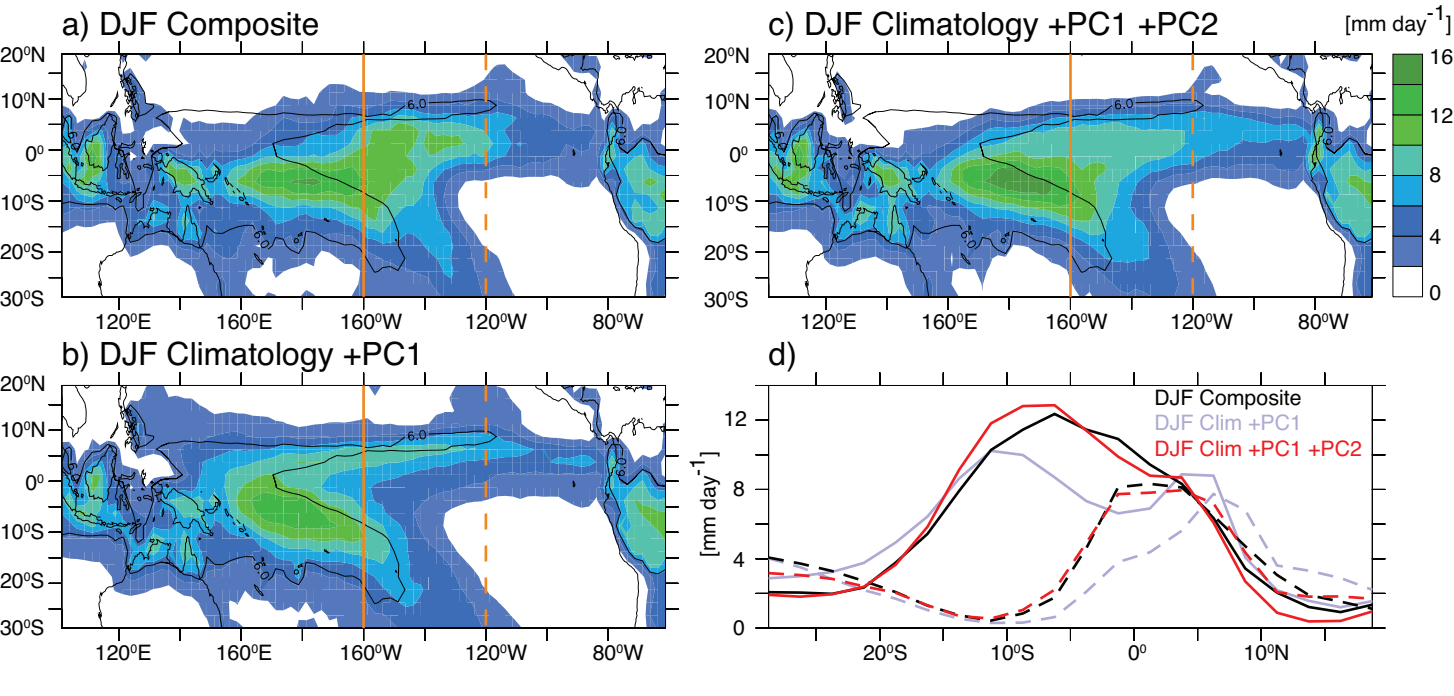
a) DJF Composite
b) DJF Climatology +PC1
c) DJF Climatology +PC2 +PC1
d)
[mm day-1]
16
12
8
4
0
6.0
20ºN
10ºN
0º
10ºS
20ºS
30ºS
120ºE
160ºE
160ºW
120ºW
80ºW
DJF Composite
DJF Clim +PC1
DJF Clim +PC1 +PC2
[mm day-1]
12
8
4
0
20ºS
10ºS
0º
10ºN